New Journal of Physics
The open access journal at the forefront of physics

Deutsche Physikalische Gesellschaft DPG IOP Institute of Physics

PAPER • OPEN ACCESS

Collective excitations and supersolid behavior of bosonic atoms inside two crossed optical cavities

To cite this article: J Lang *et al* 2017 *New J. Phys.* **19** 123027

New Journal of Physics
The open access journal at the forefront of physics

Deutsche Physikalische Gesellschaft DPG
IOP Institute of Physics

Published in partnership with: Deutsche Physikalische Gesellschaft and the Institute of Physics

PAPER

OPEN ACCESS

RECEIVED
12 July 2017

REVISED
9 October 2017

ACCEPTED FOR PUBLICATION
17 November 2017

PUBLISHED
12 December 2017

Collective excitations and supersolid behavior of bosonic atoms inside two crossed optical cavities

J Lang[1], **F Piazza**[2] **and W Zwerger**[1]

[1] Physik Department, Technische Universität München, D-85747 Garching, Germany
[2] Max-Planck Institute for the Physics of Complex Systems, Nöthnitzer Straße 38, D-01187 Dresden, Germany

E-mail: j.lang@tum.de

Keywords: symmetry breaking, superradiance, Goldstone mode, supersolidity, cavity QED, ultracold atoms, self-ordering

Abstract

We discuss the nature of symmetry breaking and the associated collective excitations for a system of bosons coupled to the electromagnetic field of two optical cavities. For the specific configuration realized in a recent experiment at ETH [1, 2], we show that, in absence of direct intercavity scattering and for parameters chosen such that the atoms couple symmetrically to both cavities, the system possesses an approximate $U(1)$ symmetry which holds asymptotically for vanishing cavity field intensity. It corresponds to the invariance with respect to redistributing the total intensity $I = I_1 + I_2$ between the two cavities. The spontaneous breaking of this symmetry gives rise to a broken continuous translation-invariance for the atoms, creating a supersolid-like order in the presence of a Bose–Einstein condensate. In particular, we show that atom-mediated scattering between the two cavities, which favors the state with equal light intensities $I_1 = I_2$ and reduces the symmetry to $\mathbf{Z}_2 \otimes \mathbf{Z}_2$, gives rise to a finite value $\sim\sqrt{I}$ of the effective Goldstone mass. For strong atom driving, this low energy mode is clearly separated from an effective Higgs excitation associated with changes of the total intensity I. In addition, we compute the spectral distribution of the cavity light field and show that both the Higgs and Goldstone mode acquire a finite lifetime due to Landau damping at non-zero temperature.

1. Introduction

The notion of a supersolid, i.e. a solid which is able to sustain dissipationless mass currents typical for superfluids, is clearly highly counterintuitive [3]. It requires that the particles in the solid can effectively move freely through quantum mechanical delocalization [4]. A conceptually simple example, suggested by Andreev and Lifshitz [5] and by Chester [6], is a quantum crystal with a finite density of defects even at zero temperature. With Bose statistics, the resulting dilute gas of defects is expected to undergo BEC at low temperatures, giving rise to a finite superfluid density and thus e.g. to a reduced moment of rotational inertia [7]. As shown by Prokof'ev and Svistunov [8], this scenario for supersolidity is in fact the generic one because superfluid states are necessarily gapless with respect to adding and removing particles. A commensurate supersolid with an integer number of particles in the unit cell, in turn, requires a fine tuned value of the density. Formally, such a state appears in the superfluid regime of the Bose–Hubbard model [9] at fixed integer densities. While such a commensurate superfluid can in principle be realized with ultracold atoms in an optical lattice [10], it is important to stress that—similar to the case of superfluid Helium on the surface of a regular crystal—this is not a supersolid in the usual sense because translation invariance is broken *externally* and not spontaneously as a result of the interactions between the particles. This differs from several proposed realizations with ultracold atoms, where dipolar [11] or Rydberg [12] interactions as well as collective light scattering [13] or spin–orbit coupling [14] give rise to crystalline order. In particular, in the latter context, the recent observation of a stripe phase at MIT [15] provides a simple example of supersolid-like order.

A quite different system in which long range positional order may coexist with superfluid behavior has been realized in recent years by studying ultracold atoms in a high finesse cavity. In the presence of a transverse laser field there is an induced interaction between the atoms which is mediated by the cavity photons [16]. The interaction is long-ranged and, beyond a critical strength λ_c of the drive, the atoms spontaneously arrange in a periodic lattice, allowing to scatter the light from the transverse field coherently into the cavity [17, 18]. This is an example of the classic Dicke–Hepp–Lieb transition to a superradiant state [19–22] and it results in a two-fold degeneracy of the periodic arrangement of the atoms. More precisely, the $\mathbf{Z}_2$ symmetry which is broken at the Dicke–Hepp–Lieb transition is associated with the relative sign of the two degenerate wave-vectors $\mathbf{q} = \pm\mathbf{k}_0$ which appear with equal weight in the standing periodic density wave described by a non-vanishing expectation value $\langle\hat{\rho}_{\mathbf{k}_0}\rangle \neq 0$ of the density operator $\hat{\rho}_{\mathbf{q}}$ ($\mathbf{k}_0$ is the externally fixed cavity wave vector). From the point of view of off-diagonal long range order, which characterizes BEC in its most general form [23], the phase beyond λ_c is one in which extensive eigenvalues of the one particle density matrix appear not only at $\mathbf{q} = 0$ but also at arbitrary multiples of $\mathbf{q} = \pm\mathbf{k}_0$, forming a fragmented condensate with a self-generated optical lattice [24, 25]. The system therefore possesses simultaneously both diagonal and off-diagonal long range order. Despite the fact that periodic order is now generated through light-field mediated interactions between the atoms, it is not a supersolid in the standard sense because it does not sustain dissipationless particle currents e.g. of the $\mathbf{q} = 0$ part of the condensate with respect to the fixed periodic density wave pattern associated with the $\pm\mathbf{k}_0$ components[3]. Moreover, due to the long range nature of the interaction the system is effectively zero-dimensional and there are no proper Goldstone modes usually associated with the breaking of a continuous translation symmetry, which are the acoustic phonons near reciprocal lattice vectors $\mathbf{q} \simeq \mathbf{G}$ [27].

Recently, a major step towards the realization of supersolid behavior with dissipationless particle transport has been taken by Léonard and coworkers at ETH in a setup involving ultracold atoms in *two crossed* cavities [1]. In this setup, a cloud of Bose-condensed atoms is enclosed in a configuration involving two optical cavities which are at a 60° angle with respect to each other. Tuning the parameters such that the atoms couple symmetrically to both cavities, this system allows to realize light-induced crystallization of the atoms which involves an arbitrary superposition of both cavity wave vectors. Within a simple two-mode description, the two discrete symmetries $\mathbf{Z}_2$ of the individual cavities can thus be combined to a continuous $U(1)$ symmetry, allowing to observe a continuous shift of the crystallization pattern [1]. Our aim in the present work is to analyze a fully microscopic model for this setup in order to study the detailed structure of the broken symmetries and the resulting spectrum of collective excitations. In particular, we will derive the associated effective dynamic Ginzburg–Landau (GL) functional for the light field in the cavity and discuss the limits in which the system indeed exhibits the breaking of a continuous translation symmetry. Beyond a detailed discussion of symmetry breaking and the subtle issue of supersolidity in this context, our results also provide a quantitative understanding of the recent measurements of the effective Goldstone and Higgs mode frequencies [2].

2. Model and symmetries

We consider the setup used for the recent experiments at ETH [1, 2]. It consists of a three dimensional cloud of bosonic atoms trapped at the intersection of the TEM_{00}-modes of two optical cavities. All photons couple the atomic ground state to the same excited state. Generalizing the formalism developed in a previous paper [24], adiabatic elimination of the excited state (which is well justified for the experimental setup) leads to an effective Hamiltonian. In the frame rotating with the driving laser ω_L it takes the following form (note that we use units in which $\hbar = 1$ throughout the paper):

$$\hat{H} = -\sum_{i=1,2} \Delta_i \hat{a}_i^\dagger \hat{a}_i + \int \mathrm{d}\mathbf{r}\, \hat{\psi}^\dagger(\mathbf{r}) \left(-\frac{\nabla^2}{2m} + \hat{V}(\mathbf{r}) \right) \hat{\psi}(\mathbf{r}). \tag{1}$$

Here, $\hat{a}_i$ is the bosonic annihilation operator of a photon in the cavity i, $\hat{\psi}(r)$ is the bosonic annihilation operator for an atom at position $\mathbf{r}$ with mass m and $\Delta_i = \omega_L - \omega_i < 0$ is the detuning of the laser from the cavity resonance. Assuming equal dipole couplings $g_1 = g_2 = g$ in both cavities, the associated single-particle potential —which still depends on the quantum state of the cavity field—is given by

$$\hat{V}(\mathbf{r}) = V_L(y) + \sum_{i=1,2} V_i(\mathbf{r})(\hat{a}_i + \hat{a}_i^\dagger) + \sum_{i,j=1,2} V_{i,j}(\mathbf{r}) \hat{a}_i^\dagger \hat{a}_j, \tag{2}$$

where V_L accounts for the pump potential while V_1 and V_2 are the potentials resulting from the interference between one cavity and the pump. They are given by

[3] Within a hydrodynamic description, such dissipationless currents would be associated with a fourth sound-like mode with linear dispersion, see [26].

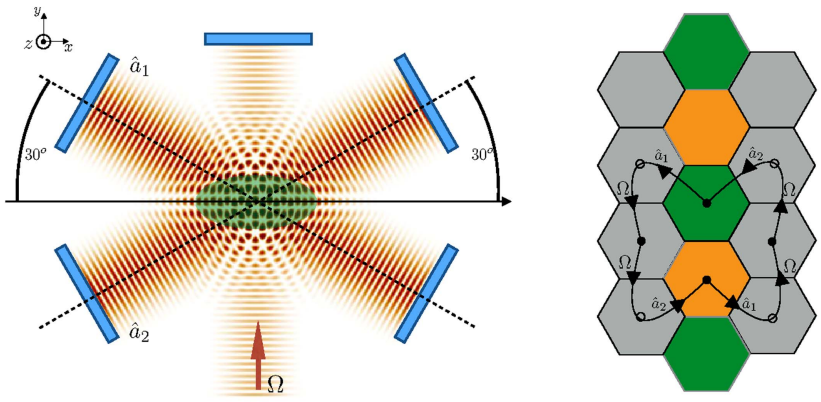

Figure 1. Left: sketch of the setup considered as implemented in the experiments of [1]. Right: momentum space in the repeated-zone scheme, where each hexagon indicates the Brillouin zone for a given band. Green zones are occupied even without cavity fields and in particular their center (Γ-point) is the only state occupied at $T = 0$. Gray zones are occupied via cavity-photon scattering and correspond to the truncation used in the $U(1)$-symmetric Hamiltonian (6). The closed curve indicates a scattering path involving two photons from each cavity. This scattering process, for which we need to include the orange zones in our Hilbert-space truncation, explicitly breaks the $U(1)$ symmetry of the full Hamiltonian (1).

$$V_L = \frac{\Omega^2}{\Delta_A}\cos^2\left(k_0 y + \frac{\pi}{2}\right),$$
$$V_1 = g\frac{\Omega}{\Delta_A}\cos\left(k_0 y + \frac{\pi}{2}\right)\cos\left(\frac{\sqrt{3}}{2}k_0 x + \frac{1}{2}k_0 y\right),$$
$$V_2 = g\frac{\Omega}{\Delta_A}\cos\left(k_0 y + \frac{\pi}{2}\right)\cos\left(\frac{\sqrt{3}}{2}k_0 x - \frac{1}{2}k_0 y\right), \tag{3}$$

where Ω is the Rabi frequency of the driving laser while $\Delta_A = \omega_L - \omega_A < 0$ is the detuning of the atomic resonance from the driving laser at frequency ω_L. Note that in the experiment under consideration [1, 2] the laser drive is far detuned ($\Omega/|\Delta_A| \approx 3 \times 10^{-4}$), which justifies the adiabatic elimination underlying the effective Hamiltonian (1). The last term in equation (2) describes the effects of direct inter- and intracavity scattering. The associated effective potential $V_{i,j}(\mathbf{r}) = \eta_i(\mathbf{r})\eta_j(\mathbf{r})$ is determined by the two mode functions

$$\eta_1(\mathbf{r}) = \frac{g}{\sqrt{|\Delta_A|}}\cos\left(\frac{\sqrt{3}}{2}k_0 x + \frac{1}{2}k_0 y\right) \quad \text{and} \quad \eta_2(\mathbf{r}) = \frac{g}{\sqrt{|\Delta_A|}}\cos\left(\frac{\sqrt{3}}{2}k_0 x - \frac{1}{2}k_0 y\right), \tag{4}$$

which correspond to the configuration shown in figure 1, where the cavity axes form a 30° angle with the x axis and lie in the x–y plane i.e. $\mathbf{k}_{1,2} = k_0(\mathbf{n}_x\cos(30°) + \mathbf{n}_y\sin(30°))$. The pump axis is along the y direction i.e. $\mathbf{k}_p = k_0\mathbf{n}_y$ and the standing wave obtained by retroreflection has a phase-shift $\pi/2$. Due to the small detuning $|\Delta_i| \ll \omega_L$ the pump and cavity modes can be taken to have the same wavelength $\lambda_0 = 2\pi/k_0$. In the following discussion we will include the leading contribution of the direct intracavity processes $\propto\eta_i(\mathbf{r})\eta_i(\mathbf{r})$ as a dispersive shift to the cavity detuning

$$\delta_{c_i} = -\Delta_i + \frac{Ng^2}{2\Delta_A} > 0. \tag{5}$$

We will however neglect contributions quadratic in $V_{i,j}(\mathbf{r})$, which are of order g^4. This is valid in the experimentally realized regime where fourth order processes due to V_1 and V_2 are more important than second order effects in $V_{i,j}$. Since intermediate states in this perturbation series carry energies $\sim E_R$ (in the superradiant phase creation of cavity photons costs very little energy), this reduces to the condition $\Omega \gg \sqrt{|\Delta_A E_R|}$ with recoil energy $E_R = k_0^2/2m$, which is well satisfied in the experiment (see also below). As the critical Rabi amplitude $\Omega_c \propto |\Delta_A|$ is decreased, close to the onset of superradiance, direct intercavity scattering will eventually be the dominant effect. The role of these processes, together with different choices of the retroreflection phase-shift, have been theoretically investigated in [28, 29].

As discussed in [1], assuming small (in a sense that will become clear later) light field intensities so that multiple scattering is suppressed, we can restrict the Hilbert space to the lowest nine momentum states $|k_x, k_y\rangle = |0, 0\rangle$, $|\pm\mathbf{k}_i \pm \mathbf{k}_p\rangle$ (see also figure 1) and truncate the Hamiltonian (1) as follows [1]:

$$\hat{H}_{\text{trunc}} = \sum_{i=1,2}\left[\delta_{c_i}\hat{a}_i^\dagger\hat{a}_i + E_+\hat{c}_{i+}^\dagger\hat{c}_{i+} + E_-\hat{c}_{i-}^\dagger\hat{c}_{i-} - \frac{g\Omega}{2\sqrt{2}\Delta_A}(\hat{a}_i^\dagger + \hat{a}_i)(\hat{c}_{i+}^\dagger\hat{c}_0 + \hat{c}_{i-}^\dagger\hat{c}_0 + \text{h.c.})\right], \tag{6}$$

where $\hat{c}^{\dagger}_{i\pm}$ excites an atom into a standing wave of wave vector $\mathbf{k}_i \pm \mathbf{k}_p$ with energy $E_{\pm} = (2 \pm 1)E_R$ and $\hat{c}_0$ removes an atom at $\mathbf{k} = 0$. Here $g\Omega/|\Delta_A|$ is the effective cavity pump strength. The truncated Hamiltonian (6) has in general a $\mathbf{Z}_2 \otimes \mathbf{Z}_2$ symmetry corresponding to the following transformation

$$(\hat{a}_1, \hat{c}_{1\pm}) \rightarrow -(\hat{a}_1, \hat{c}_{1\pm}), \tag{7}$$

$$(\hat{a}_2, \hat{c}_{2\pm}) \rightarrow -(\hat{a}_2, \hat{c}_{2\pm}). \tag{8}$$

The spontaneous breaking of either one of these discrete symmetries corresponds to a superradiant phase transition characterized by the order parameter $\langle \hat{a}^{\dagger}_i + \hat{a}_i \rangle$ or equivalently $\langle \hat{c}^{\dagger}_{i+}\hat{c}_0 + \hat{c}^{\dagger}_{i-}\hat{c}_0 + \text{h.c.} \rangle$. In the full model in real space given by equation (1), the above $\mathbf{Z}_2 \otimes \mathbf{Z}_2$ symmetry corresponds to the transformations

$$(\hat{a}_1, \mathbf{r}) \rightarrow \left(-\hat{a}_1, \mathbf{r} + \pi \frac{\mathbf{k}_1}{|\mathbf{k}_1|^2} \right), \tag{9}$$

$$(\hat{a}_2, \mathbf{r}) \rightarrow \left(-\hat{a}_2, \mathbf{r} + \pi \frac{\mathbf{k}_2}{|\mathbf{k}_2|^2} \right), \tag{10}$$

which involve a discrete spatial translation along a cavity axis. In this sense, the superradiant transition corresponds to a self-ordering of the atoms into a spatial pattern which scatters constructively into the cavity [16].

As pointed out in [1], for a symmetric choice of cavity detunings $\Delta_1 = \Delta_2$ there is an accidental $U(1)$ symmetry in the truncated Hamiltonian (6):

$$\begin{aligned}&(\hat{a}_1, \hat{c}_{1\pm}, \hat{a}_2, \hat{c}_{2\pm}) \\ &\quad \rightarrow (\hat{a}_1 \cos\theta - \hat{a}_2 \sin\theta, \hat{c}_{1\pm}\cos\theta - \hat{c}_{2\pm}\sin\theta, \hat{a}_1 \sin\theta + \hat{a}_2 \cos\theta, \hat{c}_{1\pm}\sin\theta + \hat{c}_{2\pm}\cos\theta).\end{aligned} \tag{11}$$

The signatures of the spontaneous breaking of this continuous symmetry, which corresponds to a fixed value of the relative phase θ of the two coherent cavity fields, varying randomly between different realizations, have been experimentally investigated in [1, 2]. In particular, it has been shown that the symmetry broken state possesses a collective excitation with a frequency below the experimental resolution of 100 kHz. Correspondingly the cavity fields have been observed at randomly distributed relative amplitudes with a fixed overall output intensity. Both these signatures have been interpreted as the Goldstone mode of the broken $U(1)$ symmetry.

As discussed in [1], the transformations (11) can be translated into an invariance of the potential (2) in real space. Indeed, by examining the potential (2) we see that by restricting to the subspace X defined by $k_0 y + \pi/2 = n\pi$, $n \in \mathbb{Z}$, the potential is invariant under:

$$\begin{aligned}&(\hat{a}_1, \hat{a}_2, x, y = \pi(n - 1/2)/k_0) \\ &\quad \rightarrow (\hat{a}_1 \cos\theta - \hat{a}_2 \sin\theta, \hat{a}_1 \sin\theta + \hat{a}_2 \cos\theta, x \pm 2\theta/(\sqrt{3}\,k_0), y = \pi(n - 1/2)/k_0),\end{aligned} \tag{12}$$

where the $-(+)$ sign applies for even (odd) values of n. The continuous symmetry of the Hamiltonian under rotations of the cavity field by an angle θ and a simultaneous shift of the atoms along the x-direction by $\pm 2\theta/(\sqrt{3}\,k_0)$ thus leads to supersolid-like behavior with no restoring force for translations of the atoms along the x-direction.

Now, the fact that the $U(1)$ symmetry (12) in the full model (1) is restricted to the subspace X of discretely spaced values of the y coordinate implies that this symmetry holds only approximately. The fundamental reason is that the potential (2) has no minimum on the $U(1)$-symmetric lines $y = \pi(n - 1/2)/k_0$, but rather at a position which is shifted by an amount inversely proportional to the amplitude of the state independent ac-Stark shift V_L in the effective potential. This shift appears due to interference between the two cavity fields and is therefore present for any finite number of photons in *both* cavities. The corresponding lowest-order scattering processes are depicted in figure 1 as a closed path involving two photons for each cavity, which for equal intensities $I_1 = I_2 = I$ implies that the lowest order of the explicit breaking of the $U(1)$ symmetry is proportional to I^2. It is important to note that the description of these scattering processes requires the inclusion of momentum states that are absent in the truncation used to obtain the Hamiltonian (6) (see figure 1). In the following we will discuss the consequences of the explicit $U(1)$ symmetry breaking for the supersolid-like features, which will turn out to be still approximately present in the limit of intense laser driving Ω.

To understand the physics beyond the deviations from a perfect $U(1)$-symmetry, it is convenient to use a simple effective Hamiltonian obtained by adiabatically eliminating the photons from (1). Assuming deep lattices such that we can neglect the kinetic term as well as all terms beyond $\mathcal{O}(g^2)$ from the contribution $V_{i,j}(\mathbf{r})$, the resulting effective Hamiltonian

$$\hat{H} = \int \mathrm{d}\mathbf{r}\, \hat{\psi}^{\dagger}(\mathbf{r})\hat{\psi}(\mathbf{r}) \left(V_L(\mathbf{r}) - \sum_i \frac{V_i(\mathbf{r})}{\delta_{c_i}} \int \mathrm{d}\mathbf{r}'\, V_i(\mathbf{r}')\hat{\psi}^{\dagger}(\mathbf{r}')\hat{\psi}(\mathbf{r}') \right) \tag{13}$$

for the atoms alone contains an instantaneous, cavity field induced, attractive density–density interaction of the form $-\sum_i V_i(\mathbf{r})\, V_i(\mathbf{r}')/\delta_{c_i}$ which does not decay as a function of the separation $|\mathbf{r} - \mathbf{r}'|$. Since we neglect direct

intercavity scattering, there are no interactions of higher order in the density. In the case that only a single cavity is superradiant the ground state is given by a density distributed solely within the high symmetry subspace X

$$\rho(\mathbf{r}) = \rho_0 \frac{2\pi^2}{\sqrt{3}} \delta\left(k_0 y - \frac{\pi}{2} + n\pi\right) \delta\left(k_0 x - \frac{\mp\pi + 4\pi m}{2\sqrt{3}}\right), \; n, m \in \mathbb{Z} \tag{14}$$

with $\rho_0 = N/V$. Here, the minus sign implies superradiance in cavity 1 ($\alpha_1 = \langle \hat{a}_1 \rangle \neq 0$) while the plus sign corresponds to a finite expectation value of $\alpha_2 = \langle \hat{a}_2 \rangle$. The energy density of both states is given by $\epsilon = \frac{\Omega^2}{\Delta_A}(1 + c)$, with $c = Ng^2/\delta_{c_i}|\Delta_A|$ a dimensionless positive constant which is much less than one for typical experimental parameters. For two identical cavities $\delta_{c_i} = \delta_c$ and therefore $\alpha = \alpha_i$, this is, however, not in the ground state manifold which instead contains for example the density profile

$$\rho(\mathbf{r}) = \rho_0 \frac{2\pi^2}{\sqrt{3}} \delta\left(k_0 x - \frac{2n\pi}{\sqrt{3}}\right) \sum_{\sigma=\pm} \delta\left(k_0 y + 2\sigma \arcsin\left(\sqrt{\frac{1 + 4c - d(c)}{6c}}\right) + 2\pi m\right), \tag{15}$$

with $n, m \in \mathbb{Z}$ and $d(c) = \sqrt{1 + 2c + 4c^2}$. This density distribution slightly frustrates the potential V_L induced by the ac-Stark shift of the atoms and shifts the densities away from the X subspace. It therefore slightly breaks $U(1)$ invariance in the atomic density and locks the relative cavity phases. The small energy difference between state (15) and state (14) is given by

$$\Delta\epsilon = -\frac{\Omega^2}{\Delta_A}\left[1 + c + \frac{1}{27c^2}(1 + 4c - d(c))(1 - 2c - d(c))(2 + 2c + d(c))\right] \approx \frac{\Omega^2 c^2}{4\Delta_A} < 0. \tag{16}$$

As will be discussed below, this energy determines the scale of the effective Goldstone mass. Resubstituting either one of these density profiles into the cavity equations of motion we obtain $|\alpha| = \sqrt{I} \approx N\Omega g/|\Delta_A|\delta_c$ to leading order in c, which shows that in the deep lattice limit the critical coupling strength λ_c vanishes. Since kinetic energy contributions have been neglected, the Goldstone mass has an upper bound

$$m_G = \frac{\sqrt{-\Delta\epsilon}}{\alpha} \lesssim \frac{\delta_c\sqrt{-\Delta_A I}}{\Omega N} = \frac{g}{\sqrt{-\Delta_A}}. \tag{17}$$

Physically the Goldstone mass m_G arising from the finite energy scale $\Delta\epsilon$ associated with the breaking of the $U(1)$ symmetry describes the azimuthal curvature of the GL potential, which will be discussed in more detail in section 4. As expected according to the argument based on the scattering processes illustrated in figure 1, $\Delta\epsilon \propto |\alpha^4| = I^2$. The explicit symmetry breaking $\Delta\epsilon$ due to the latter scattering processes has actually the same scaling with intensity as the one which would result from direct intercavity scattering (not involving the pump Ω), which we neglected in our model (1). As mentioned before, this is justified in the experimentally realized limit $\Omega/\sqrt{|\Delta_A E_R|} \gg 1$, where direct intercavity scattering is suppressed with respect to the processes shown in figure 1. In particular, the fact that we can neglect all contributions from the last term in (2) beyond the simple dispersive shift has no influence on the $U(1)$ invariance in subspace X. Even including all contributions from the last term in (2), the explicit breaking of the $U(1)$ symmetry is still caused by the fact that the global potential minimum for the atoms lies outside the subspace X.

3. Effective action and phase diagram

In order to compute the phase diagram and the experimentally accessible spectrum of the cavity light field, we extend the effective equilibrium path-integral approach developed in [24] for a single-cavity configuration. We derive an effective action for the cavity degrees of freedom by exactly integrating out the atoms. The action splits into a mean-field (MF) plus a fluctuation (FL) part. The latter will be discussed in detail in section 5 below. As shown in [24], this action becomes exact in the thermodynamic limit due to the infinite-range interactions. By separating the coherent part of cavity fields $\alpha_i = \langle \hat{a}_i \rangle$ as well as the atom field $\phi(\mathbf{r}) = \langle \hat{\psi}(\mathbf{r}) \rangle$ (which corresponds to the condensate fraction) we obtain the effective action

$$S_{\text{eff}}[a^*_{1,2}, a_{1,2}] = S^{(\text{MF})}_{\text{eff}} + S^{(\text{FL})}_{\text{eff}}[a^*_{1,2}, a_{1,2}]. \tag{18}$$

The leading MF action reads

$$S^{(\text{MF})}_{\text{eff}} = -\sum_{i=1,2} \Delta_i |\alpha_i|^2 + \text{Tr} \ln[G^{-1}] + \int \mathrm{d}\mathbf{r}\, \phi^*(\mathbf{r}) \left[-\frac{\nabla^2}{2m} + V_{\text{sp}}(\mathbf{r}) - \mu\right] \phi(\mathbf{r}). \tag{19}$$

It involves an effective c-number single-particle potential $V_{\text{sp}}(\mathbf{r}) = \hat{V}(\mathbf{r})|_{\hat{a}_i \to \alpha_i}$ felt by the atoms in which the light field operators are replaced by their coherent state expectation values. The atom propagator defined by

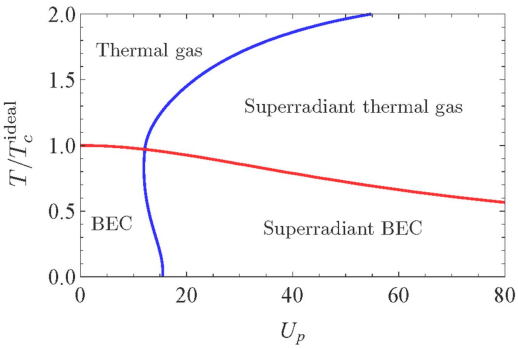

Figure 2. Phase diagram in the U_p–T plane for parameters $\Delta_2 = \Delta_1$, $\epsilon_R = 8, n = 1, \lambda = 2.8$. To the right of the blue line the system is in a superradiant state with equal intensity in both cavities, below the red line a finite fraction of the atoms is condensed.

$$G^{-1}_{n,n'}(\mathbf{r},\mathbf{r}') = \left[-\mathrm{i}\omega_n - \frac{\nabla^2}{2m} + V_{\mathrm{sp}}(\mathbf{r}) - \mu\right]\delta_{n,n'}\delta(\mathbf{r}-\mathbf{r}'), \tag{20}$$

where the integers $n,\ n'$ label the Matsubara space with frequencies $\omega_n = 2\pi n k_B T$, k_B is the Boltzmann constant and T the temperature of the system. In equation (19) the trace $\mathrm{Tr} = \int \mathrm{d}\mathbf{r}\sum_n$ is taken over coordinate and Matsubara space and μ is the atomic chemical potential.

The saddle-point associated with the MF action defines a closed system of equations:

$$\begin{aligned} -\Delta_i\alpha_i + \int \mathrm{d}\mathbf{r}\,\frac{\partial V_{\mathrm{sp}}(\mathbf{r})}{\partial\alpha_i^*}[|\phi(\mathbf{r})|^2 + \rho(\mathbf{r})] = 0, \quad i = 1, 2 \\ \left(-\frac{\nabla^2}{2m} + V_{\mathrm{sp}}(\mathbf{r}) - \mu\right)\phi(\mathbf{r}) = 0 \\ \int \mathrm{d}\mathbf{r}\,(|\phi(\mathbf{r})|^2 + \rho(\mathbf{r})) = N, \end{aligned} \tag{21}$$

with the condensed $\rho_0(\mathbf{r}) = |\phi(\mathbf{r})|^2$ and non-condensed $\rho(\mathbf{r}) = \langle\hat\psi^\dagger(\mathbf{r})\hat\psi(\mathbf{r})\rangle - \rho_0(\mathbf{r}) = \sum_\ell n_b(\epsilon_\ell - \mu)|v_\ell(\mathbf{r})|^2$ atom density. Here $v_\ell(\mathbf{r})$ are the eigenvectors of the single-atom Hamiltonian with potential $V_{\mathrm{sp}}(\mathbf{r})$ with eigenvalue ϵ_ℓ, and $n_b(x) = (\exp(x/k_BT) - 1)^{-1}$ is the Bose–Einstein distribution. The second equation in (21) is the Gross–Pitaevskii equation for the condensate wavefunction while the third equation fixes the chemical potential. We stress that both $\rho(\mathbf{r})$ and $V_{\mathrm{sp}}(\mathbf{r})$ depend on the cavity coherent parts $\alpha_{1,2}$. It is convenient to introduce dimensionless quantities, which we define by

$$\delta_c = \min_i(\delta_{c_i}),\ n = \frac{\rho_0}{(m\delta_c)^{3/2}},\ U_p = \frac{\Omega^2}{|\Delta_A|\delta_c},\ \lambda = \frac{\Omega g\sqrt{N}}{|\Delta_A|\delta_c},\ \epsilon_R = \frac{E_R}{\delta_c}. \tag{22}$$

Moreover, we measure temperatures in units of the critical temperature of an ideal Bose gas $T_c^{\mathrm{ideal}} = 2\pi\delta_c(n/\zeta(3/2))^{2/3}$ at the given average density n and with ζ the Riemann zeta function. We furthermore rescale $\alpha \to \alpha/\sqrt{N}$ in the remainder of this paper and in all figures.

As discussed in the previous section, the Hamiltonian (1) possesses the $\mathbf{Z}_2 \otimes \mathbf{Z}_2$ symmetry defined by equation (9). The corresponding order parameters are the two real quantities

$$X_{1,2} = \langle\hat{\mathrm{X}}_{1,2}\rangle = \langle\hat a_{1,2} + \hat a_{1,2}^\dagger\rangle = 2\,\mathrm{Re}(\alpha_{1,2}). \tag{23}$$

A finite expectation value $X_i \neq 0$ creates the effective one-body potential V_i, which results in an atomic density wave. Thus equivalent order parameters can be defined by the density components

$$\begin{aligned} \rho_{1,2} &= \int \mathrm{d}\mathbf{r}\,\cos(\mathbf{k}_p\cdot\mathbf{r})\cos(\mathbf{k}_{1,2}\cdot\mathbf{r})\langle\hat\psi^\dagger(\mathbf{r})\hat\psi(\mathbf{r})\rangle \\ &= \int \mathrm{d}\mathbf{r}\,\cos(\mathbf{k}_p\cdot\mathbf{r})\cos(\mathbf{k}_{1,2}\cdot\mathbf{r})(|\phi(\mathbf{r})|^2 + \rho(\mathbf{r})). \end{aligned} \tag{24}$$

Additionally, we have the Bose–Einstein condensation transition described by the $U(1)$ order parameter $\phi(\mathbf{r})$.

We first investigate the interplay between the superradiant transition and the Bose–Einstein condensation by solving the MF equations (19) as a function of temperature T and driving strength U_p. The corresponding phase diagram, which is qualitatively the same as the one for the single-cavity case considered in [24] is shown in figure 2[4]. With growing values of the coupling strength U_p the atomic gas becomes increasingly confined to the

[4] We choose $E_R = 8\delta_c$ for our computations. This is much larger than the experimental values $E_R \sim \delta_c/100$ of the recoil energies, which would increase the numerical effort considerably without changing the qualitative physics.

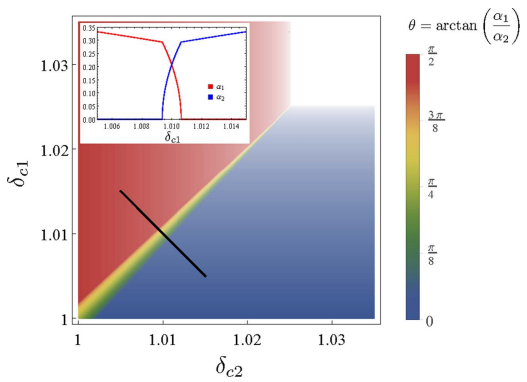

Figure 3. Phase diagram in the δ_{c_1}–δ_{c_2} plane. The color scale indicates the angle in θ in the α_1–α_2 plane. Inset: cavity amplitudes along the black line indicated on the phase diagram. The parameters used are $T = 0$, $\lambda = 2.82$, $\eta = 4$ and $\epsilon_R = 8$.

minima of the effective single-particle potential, which results in an enhancement of the kinetic energy and therefore a reduction of the critical temperature for Bose–Einstein condensation T_c. Beyond a critical coupling strength U_{p_c} (or equivalently λ_c) the atoms spontaneously arrange into a spatially ordered configuration, resulting in a superradiant backscattering of light into the cavity. This Dicke–Hepp–Lieb transition as indicated by the blue line in figure 2 can be found both with and without a condensate fraction. Additionally, a finite, but small, temperature can enhance the tendency towards superradiance, as can be seen from the decrease of the critical driving strength for increasing temperatures at $T \lesssim T_c^{\text{ideal}}$.

The phase diagram of figure 2 is computed for a symmetric cavity configuration i.e. for equal detunings $\Delta_1 = \Delta_2$, implying that in the superradiant phase both cavities are equally occupied with order parameters $\alpha_1 = \alpha_2$. For a comparison with the experimental results we also compute the zero temperature phase diagram in the δ_{c_1}–δ_{c_2} plane, which is shown in figure 3. Apart from the superradiant phases with only one nonzero cavity field i.e. $\alpha_{1,2} \neq 0$, $\alpha_{2,1} = 0$ we observe a narrow region around the diagonal $\Delta_1 = \Delta_2$ where both $\mathbf{Z}_2$ symmetries are broken i.e. $\alpha_1 \neq 0$, $\alpha_2 \neq 0$. Within this small region of the phase diagram the two cavity order parameters are not equal, as quantified by the color scale in figure 3, indicating the value of the angle θ in the α_1–α_2 plane (see also figure 4), defined as

$$\theta = \arctan\left(\frac{\alpha_1}{\alpha_2}\right),$$

which equals the $U(1)$-parameter of equation (12).

This region exists due to the fact that the $U(1)$ symmetry of equation (12) is not perfectly realized. In particular, the size of the region is set by the value of the Goldstone mass. Using equation (17) and the experimental parameters $\Omega^2/|\Delta_A| = 38\ E_R$, $g^2/|\Delta_A| = 5 \times 10^{-4}\ E_R$ and $|\Delta| = 10^3\ E_R$ [1], one obtains $|\Delta\epsilon| \sim m_G^2\alpha^2 \sim 0.1\ E_R$, consistent with the experimental result $|\Delta\epsilon| < 10\ E_R$.

4. GL potential for the cavity fields and role of cavity losses

In order to investigate the approximate $U(1)$ symmetry of our model in more detail, we compute the full GL potential corresponding to the MF equations (21). The resulting effective potential in the α_1–α_2 plane is shown in figure 4, both for an asymmetric and the perfectly symmetric choice of detunings, at zero and finite temperature.

The asymmetric case for $T = 0$ is picked such that we are in the single-cavity superradiant phase and the GL potential has indeed two minima at angles $\theta = 0, \pi$ when cavity 1 is preferred, or $\theta = \pm\pi/2$ when cavity 2 is preferred. The asymmetric case for $T = 0.9T_c$ is instead picked such that we still are in the coexistence region where both cavities are occupied and where the GL potential has four minima. One of those is shown at an angle slightly below $\theta = \pi/4$, connected by reflection symmetry with respect to the origin.

On the contrary, for $\Delta_1 = \Delta_2$ the GL potential shows four degenerate minima at $\theta = \pm\pi/4, \pm 3\pi/4$. Since a $U(1)$ symmetric potential would show a degenerate minimum on a whole circle, we see that the extent to which this symmetry is explicitly broken is measured by the azimuthal curvature of the potential about anyone of the four minima, which determines the square of the effective Goldstone mass. The latter, together with the associated effective Higgs mass, which corresponds to the square root of the curvature in the radial direction, is shown in figure 5 across the superradiant phase transition at zero and at finite temperature. In the disordered phase there is only a single collective mode in the radial direction with a mass vanishing at the critical point.

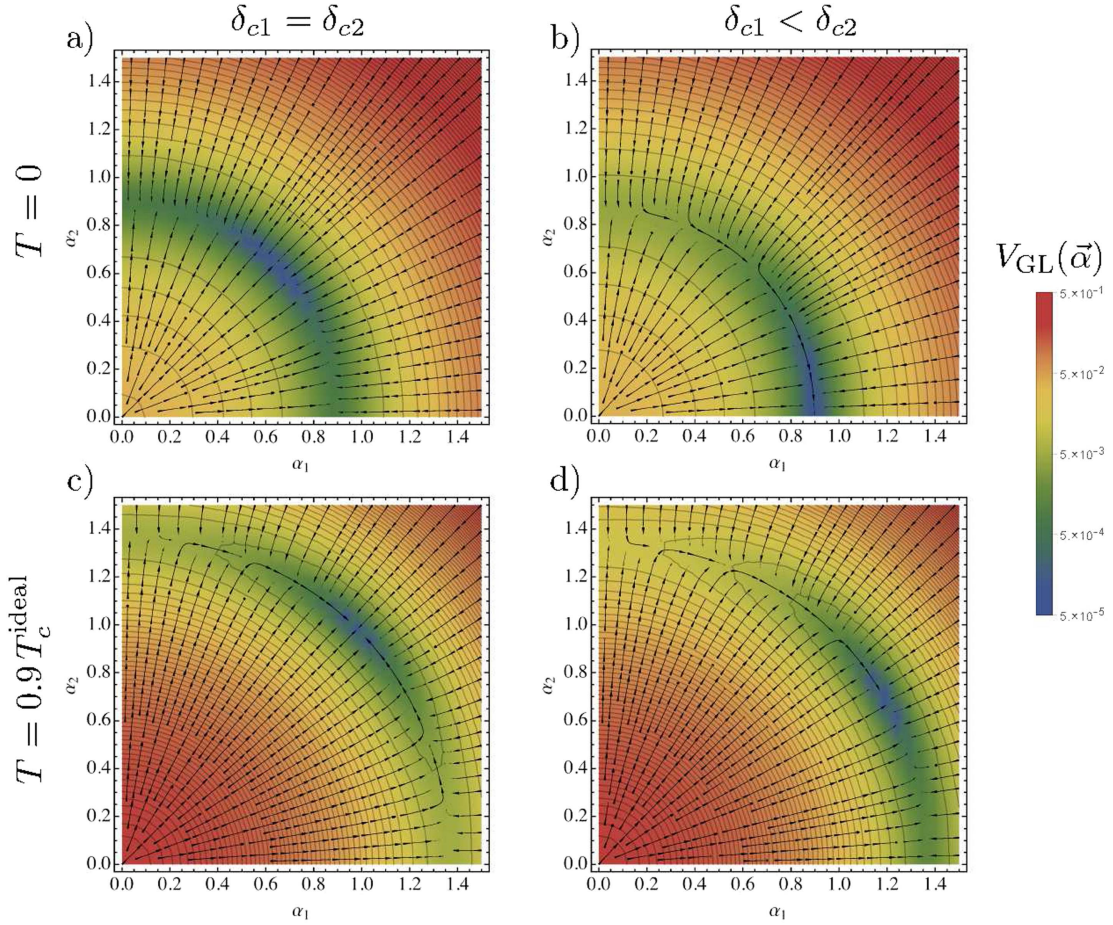

Figure 4. Ginzburg–Landau potential V_{GL} as a function of the cavity amplitudes. Arrows indicate the gradient. (a), (b) are for $T = 0$ while (c), (d) for $T = 0.9T_c^{\text{ideal}}$. (a) and (c) correspond to a symmetric configuration $\delta_{c_1} = \delta_{c_2}$, while (b) and (d) correspond to $\delta_{c_2} = 1.01\delta_{c_1}$. The remaining parameters are $\eta = 10$, $\epsilon_R = 8$ as well as $\lambda = 3$ in (a), (b) and $\lambda = 2.7$ in (c), (d). Notice the small curvature along the azimuthal direction.

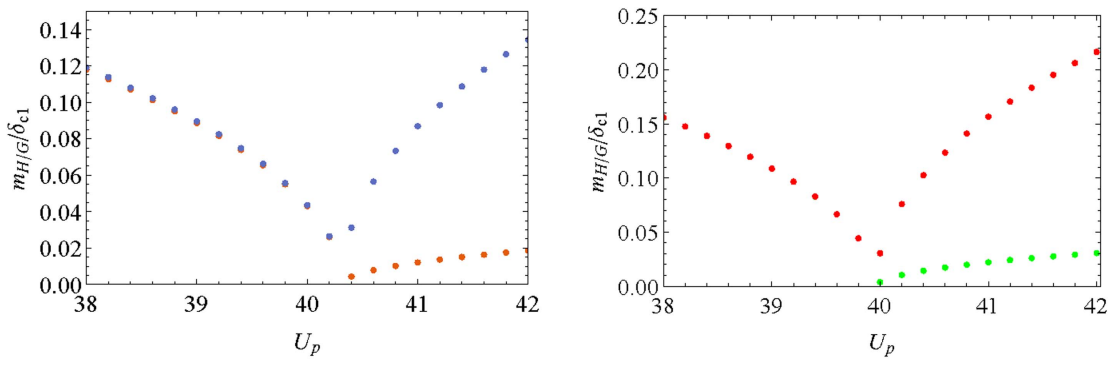

Figure 5. Goldstone and Higgs mass across the superradiant transition at $T = 0$ (left) and $T = 0.5T_c^{\text{ideal}}$ (right). Parameters are the same as in figure 2 apart from $\lambda = 2.278$.

Beyond this point Goldstone and Higgs mass separate, the latter growing much faster while the former remains at least one order of magnitude smaller. By expanding the GL potential one can show that the Goldstone mass close to the critical point is proportional to $\sqrt{\alpha_1\alpha_2}$, in accordance with the arguments discussed in section 2. Moreover, the ratio between Goldstone mass and Higgs mass is inversely proportional to the drive strength, so that for the strong drive employed in experiment and considered in figure 5 we find a large separation between the Higgs and the Goldstone mass.

The qualitative behavior and the ratio of the Goldstone to Higgs mass shown in figure 5 is consistent with the experimental results of [2]. By contrast, the presence of a well-defined minimum in the GL potential in the range

$0 < \theta < \pi/2$ of figure 4 is not compatible with the experimental finding [1] that θ is homogeneously distributed in this range. However, we can reconcile our prediction with the experiment by adding the noise induced by cavity losses to the picture. The probability of escaping the minimum and delocalizing across the circle in figure 4 is given by $P_{\mathrm{deloc}} \approx \exp(-\sqrt{N_{\mathrm{ph}}}\Delta V/\kappa)$, where $\Delta V \propto \alpha^4 \propto |\lambda - \lambda_c|^2$ is the depth of the minimum while κ is the cavity loss rate. Note that the noise is suppressed by a factor $1/\sqrt{N_{\mathrm{ph}}}$ if we assume a coherent cavity field. With the experimental value $\kappa/2\pi \sim 200$ kHz and with $\Delta V \simeq |\Delta\epsilon|$ which is determined by the square of the Goldstone mass according to the first equality in equation (17), typical values $N_{\mathrm{ph}} = |\alpha|^2 \sim 100$ lead to an escape probability of $P_{\mathrm{deloc}} \simeq \exp(-0.02) \simeq 0.98$. We stress that our estimate for ΔV is an upper bound and thereby our escape probability provides a lower bound. A critical test for this scenario of a restoration of the $U(1)$ symmetry by cavity loss induced noise, is that with an increasing number of intracavity photons the escape probability is expected to decrease exponentially like

$$P_{\mathrm{deloc}} \propto \exp(-N_{\mathrm{ph}}^{5/2}). \tag{25}$$

5. Effective action for low-energy excitations

In this final section we will discuss the nature of the low-energy excitations of the cavity field in the superradiant phase. For this purpose we expand the effective action derived in section 3 up to quadratic order about the minima of the MF potential discussed in section 4. The resulting time-dependent deviations $a_i(\tau)$ can be expanded in terms of discrete Fourier-coefficients $a_{i,n}$ which determine the spectrum of light field fluctuations in the cavity. Thus, the effective Goldstone and Higgs mode appear explicitly, allowing to compute both their masses discussed above and—moreover—their damping or inverse lifetime which appears at finite temperature.

As described in section 3, in the thermodynamic limit the action (18) can be expanded up to quadratic order in the fluctuations. Since the coupling between atoms and the imaginary part of the cavity fields results solely in a dispersive shift, we can integrate out the imaginary part, generating only even powers in ω_n. At zero temperature the fluctuation part in dimensionless units is then given by

$$\begin{aligned} S_{\mathrm{eff}}{}^{(\mathrm{FL})}[a^R_{1,2}]|_{T=0} = &\sum_{n\neq 0}\sum_{i=1,2}\{(\omega_n^2+1)a^R_{i,n}a^R_{i,-n} \\ &+4\sum_{j=1,2}\sum_{l}\frac{1}{\mathrm{i}\omega_n-\epsilon_l(0)}\langle\Psi_0(0)\left|\frac{\partial V_{\mathrm{sp}}}{\partial\alpha_i^*}\right|\Psi_l(0)\rangle\langle\Psi_l(0)\left|\frac{\partial V_{\mathrm{sp}}}{\partial\alpha_j^*}\right|\Psi_0(0)\rangle a^R_{i,n}a^R_{j,-n}\Big\}, \end{aligned} \tag{26}$$

where a_i^R is a real part of the cavity field and $|\Psi_l(k)\rangle$ is the atomic wave function with quasi-momentum k and band index l. This expression describes the scattering of atoms from the condensate to the Γ-point of an excited band in second order perturbation theory. Since these processes are far off-resonant with respect to the low energy excitations in the photon fields, they do not give rise to damping. The associated spectral functions are thus perfectly sharp. The picture gradually changes with increasing temperature, when more and more atoms occupy states near the edge of the Brillouin zone, where low energetic photons can be scattered resonantly. This effect can be accounted for by generalizing the effective action through the inclusion of thermally occupied states

$$\begin{aligned} S^{(\mathrm{FL})}_{\mathrm{eff}}[a^R_{1,2}] &= n_0 S^{(\mathrm{FL})}_{\mathrm{eff}}[a^R_{1,2}]|_{T=0} \\ &+\sum_{j=1,2}\sum_{m,l}V\int\frac{\mathrm{d}^3k}{4\pi^3}\langle\Psi_m(k)\left|\frac{\partial V_{\mathrm{sp}}}{\partial\alpha_i^*}\right|\Psi_l(k)\rangle\langle\Psi_l(k)\left|\frac{\partial V_{\mathrm{sp}}}{\partial\alpha_j^*}\right|\Psi_m(k)\rangle\frac{n_b(\epsilon_m(k))-n_b(\epsilon_l(k))}{\mathrm{i}\omega_n+\epsilon_m(k)-\epsilon_l(k)}a^R_{i,n}a^R_{j,-n} \\ &\equiv\sum_{n\neq 0}\sum_{i,j}\mathcal{G}(\omega_n)_{i,j}a^R_{i,n}a^R_{j,-n}, \end{aligned} \tag{27}$$

where n_0 is the condensate fraction. An important point is that, both at $T = 0$ and at finite temperature, the action involves only the real parts of the cavity fields and is thus an even function of ω. Therefore, it contains no linear terms of the form $\mathrm{i}\hbar a^R(t)\partial_t a^R(t)$ which would give rise to dynamics involving a reversible first order time derivative, where no proper Higgs mode exists [30]. Since the matrix elements respect the symmetry of the mean field action, the fluctuations can be diagonalized in terms of Goldstone and Higgs modes $a_G = -\sin\theta a_1^R + \cos\theta a_2^R$ and $a_H = \cos\theta a_1^R + \sin\theta a_2^R$. Upon expanding to second order in the frequency, we thus obtain the action

$$S^{(\mathrm{FL})}_{\mathrm{eff}}[a_G, a_H] \approx (Z_G\omega_n^2 + m_G^2)a_{G,n}a_{G,-n} + (Z_H\omega_n^2 + m_H^2)a_{H,n}a_{H,-n} \tag{28}$$

with numerical coefficients that fulfill $m_G \ll m_H$, as well as $Z_{G,H} - 1 = \mathcal{O}(m_{G,H}/\epsilon_R)$ at small temperatures. From this action the existence of a (approximately) gapless Goldstone mode together with a strongly gapped Higgs mode is apparent.

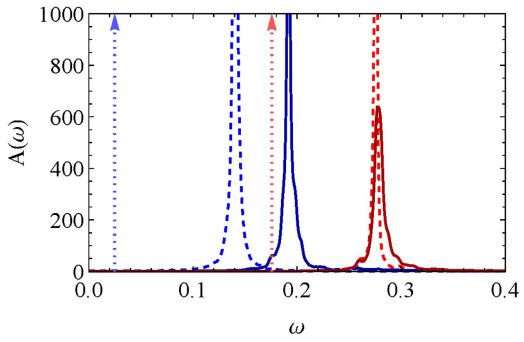

Figure 6. Low-energy excitation spectrum in the η–ω plane showing the Goldstone and Higgs peak with finite width close to the critical point. The temperatures and coupling strengths λ in order of increasing color saturation are $\{T,\ \lambda\} = \{0,\ 2.2\}$ (dotted arrows), $\{0.5,\ 2.3\}$ (dashed line) and $\{0.9,\ 2.2\}$ for the solid line.

As anticipated, at finite temperatures the Goldstone and Higgs modes experience losses via resonant Landau damping processes where a photon scatters against an atom while conserving energy and momentum. The resulting lifetimes as well as the masses of both excitations can be obtained from the spectral function $A(\omega) = 2\mathcal{J}\mathcal{G}(-\mathrm{i}\omega + 0^+)$ which can be measured via pump–probe experiments. The resulting sectra are shown in figure 6 for different temperatures[5]. For finite temperatures, there is additional structure in the tails of the Goldstone and Higgs peaks, which arises from van-Hove singularities at the edges of the Brillouin zones.

As shown in figure 6, the Goldstone mass increases drastically with temperature, an effect that cannot be observed in figure 5 for the mass obtained from the curvature of the mean field action at the global minimum. This is because in our expansion in fluctuations about the potential minima we do not allow atoms to redistribute. We are therefore effectively computing the behavior of photonic excitations at 'high' frequencies with respect to the timescale of atomic redistribution. The inclusion of atomic redistribution beyond mean field would require a non-equilibrium approach like the one employed in [31]. This would allow to interpolate smoothly between the high frequency mass, as determined in $A(\omega)$, and low frequency mass, obtained from the MF potential. However, since the atomic redistribution time is extensive in the number of atoms [31], we expect the Goldstone mass experimentally observable in large systems to correspond to the high-frequency mass measured by the spectral function.

The spectral function exhibits two distinct peaks which possess a nontrivial frequency but no momentum dependence. This is a consequence of the fact that the present double-cavity system is still an effectively zero-dimensional one. As a result, it does not give rise to a genuine spectrum of Goldstone modes usually associated with supersolids, where gauge and translation symmetry are broken simultaneously in a system with short range interactions. For such a genuine supersolid, the total free energy can be written as an integral over a spatially varying free energy density $f(T,\ n,\ \mathbf{v}_s,\ \underline{u})$ which involves thermodynamic variables which vary continuously in space. In particular, the simultaneous presence of broken translation and gauge invariance leads to two additional contributions in the differential of the free energy density

$$\mathrm{d}f|_{T,n} = \mathbf{j}_s \cdot \mathrm{d}\mathbf{v}_s + \mathrm{Tr}\ \underline{\sigma} \cdot \mathrm{d}\underline{u}. \tag{29}$$

As discussed by Liu within a hydrodynamic approach [26], the term proportional to the superfluid current density $\mathbf{j}_s$ and its conjugate variable, the superfluid velocity $\mathbf{v}_s = \frac{\hbar}{m}\nabla\phi$, results in a persistent mass flow for generic supersolids or dissipationless entropy flow in the absence of defects. Similarly, for the generic case of short range interactions where the stress tensor $\underline{\sigma}$ is linearly proportional to the strain tensor $\underline{u}$, the second contribution gives rise to phonons whose frequency $\omega(\mathbf{q}) \sim |\mathbf{q}|$ vanishes linearly with the wave vector. Due to $\omega(\mathbf{q}) = \omega(\mathbf{q} + \mathbf{G})$ for regular crystals, this entails a vanishing Goldstone mass $\omega(\mathbf{q} = \mathbf{G}) = 0$ at reciprocal lattice vectors as a signature of the spontaneous breaking of translation invariance [27]. In the present system such a Goldstone mode also exists for the motion of atoms in the limit where m_G can be neglected. It is associated with the shift along the x-direction discussed in equation (12) and leads to $\omega(\mathbf{G}) = 0$ for all reciprocal lattice vectors $\mathbf{G} = n\mathbf{k}_1 + m\mathbf{k}_2$ with $n,\ m \in \mathbb{Z}$. In particular the transverse acoustic phonon at $n = -m = \pm 1$ corresponds to the translation described in equation (12), which is related to the indirect exchange of a photon between the two cavities. In contrast to the standard situation, however, where the phonon frequencies approach zero continuously as $\mathbf{q}$ approaches 0, the long ranged nature of the interactions give rise to a finite energy gap at any $\mathbf{q} \neq \mathbf{G}$. The Goldstone mode thus exists only at isolated points in momentum space, with all other momenta being gapped.

[5] Note that up to leading order in the frequency expansion the lifetime of the modes is infinite and we need to use the full action (27) in order to introduce damping.

6. Conclusions

In summary, we have studied the nature of broken symmetries, the effective GL potential and the spectrum of the light field in the double cavity setup realized recently at ETH [1, 2]. It has been shown that the emergent $U(1)$ invariance for symmetrically coupled cavities is slightly broken by higher order photon scattering processes. We have determined an upper bound for the resulting mass of the effective Goldstone mode which is consistent with the experimental results [2]. In addition, it has been shown that the ratio m_G/m_H between the Goldstone and Higgs mass vanishes in the limit of large driving amplitudes. As an experimentally testable prediction, we have determined the cavity noise induced escape probability from the global minimum of the effective potential as a function of the intracavity photon occupation which might be used for an indirect measurement of the Goldstone mass. Finally, the issue of dissipationless transport of particles in the double cavity supersolid has been discussed carefully and has been compared to the case of genuine supersolids, where this is associated with an additional true Goldstone mode.

Acknowledgments

WZ would like to thank the Quantum Optics group at ETH for the great hospitality and for numerous discussions during a sabbatical, where this work has been started. We are grateful to Andrea Morales and Julian Léonard for careful reading and comments on the manuscript.

References

[1] Léonard J, Morales A, Zupancic P, Esslinger T and Donner T 2017 *Nature* **543** 87–90
[2] Léonard J, Morales A, Zupancic P, Donner T and Esslinger T 2017 arXiv:1704.05803
[3] Boninsegni M and Prokof'ev N V 2012 *Rev. Mod. Phys.* **84** 759–76
[4] Yang C N 1962 *Rev. Mod. Phys.* **34** 694–704
[5] Andreev A F and Lifshitz M I 1969 *Sov. Phys.—JETP* **29** 1107
[6] Chester G V 1970 *Phys. Rev.* A **2** 256–8
[7] Leggett A J 1970 *Phys. Rev. Lett.* **25** 1543–6
[8] Prokof'ev N and Svistunov B 2005 *Phys. Rev. Lett.* **94** 155302
[9] Fisher M P A, Weichman P B, Grinstein G and Fisher D S 1989 *Phys. Rev.* B **40** 546–70
[10] Greiner M, Mandel O, Esslinger T, Hansch T W and Bloch I 2002 *Nature* **415** 39–44
[11] Giovanazzi S, O'Dell D and Kurizki G 2002 *Phys. Rev. Lett.* **88** 130402
[12] Henkel N, Nath R and Pohl T 2010 *Phys. Rev. Lett.* **104** 195302
[13] Ostermann S, Piazza F and Ritsch H 2016 *Phys. Rev.* X **6** 021026
[14] Li Y, Martone G I, Pitaevskii L P and Stringari S 2013 *Phys. Rev. Lett.* **110** 235302
[15] Li J R, Lee J, Huang W, Burchesky S, Shteynas B, Top F Ç, Jamison A O and Ketterle W 2017 *Nature* **543** 91–4
[16] Ritsch H, Domokos P, Brennecke F and Esslinger T 2013 *Rev. Mod. Phys.* **85** 553–601
[17] Baumann K, Guerlin C, Brennecke F and Esslinger T 2010 *Nature* **464** 1301–6
[18] Black A T, Chan H W and Vuletić V 2003 *Phys. Rev. Lett.* **91** 203001
[19] Dicke R H 1954 *Phys. Rev.* **93** 99–110
[20] Hepp K and Lieb E H 1973 *Ann. Phys., NY* **76** 360–404
[21] Wang Y K and Hioe F T 1973 *Phys. Rev.* A **7** 831–6
[22] Nagy D, Kónya G, Szirmai G and Domokos P 2010 *Phys. Rev. Lett.* **104** 130401
[23] Penrose O and Onsager L 1956 *Phys. Rev.* **104** 576–84
[24] Piazza F, Strack P and Zwerger W 2013 *Ann. Phys., NY* **339** 135–59
[25] Lode A U J and Bruder C 2017 *Phys. Rev. Lett.* **118** 013603
[26] Liu M 1978 *Phys. Rev.* B **18** 1165–76
[27] Wagner H 1966 *Z. Phys.* **195** 273–99
[28] Safaei S, Miniatura C and Grémaud B 2015 *Phys. Rev.* A **92** 043810
[29] Gopalakrishnan S, Shchadilova Y E and Demler E 2017 arXiv:1707.03907
[30] Pekker D and Varma C 2015 *Ann. Rev. Condens. Matter Phys.* **6** 269–97
[31] Piazza F and Strack P 2014 *Phys. Rev.* A **90** 043823